Korean J. Chem. Eng., **29**(10), 1453-1458 (2012)
DOI: 10.1007/s11814-012-0026-z

Elucidation of morphological and optoelectronic properties of highly crystalline chalcopyrite ($CuInSe_2$) nanoparticles synthesized via hot injection route

Umme Farva*,‡, Mahmood Alam Khan, and Chinho Park*,†**

*School of Chemical Engineering, Yeungnam University, Gyeongsan 712-749, Korea
**Research Center for Solar Energy Chemistry, Osaka University, 1-3, Machikaneyama, Toyonaka, Osaka 560-8531, Japan
(*Received 28 January 2012 • accepted 29 February 2012*)

Abstract–$CuInSe_2$ (CIS) nanoparticles have been prepared by the hot-injection method with sizes ~25 nm, and the thermal annealing influence on the size, morphology and optoelectronic properties of crystalline $CuInSe_2$ nanoparticles has been elucidated. Microstructural analysis of synthesized nanoparticles was performed by various characterization methods including high-resolution transmission electron microscopy (HR-TEM), Scanning TEM (STEM), X-ray diffraction, X-ray photoelectron spectroscopy (XPS) and photoluminescence (PL) spectroscopy. The fast Fourier transform (FFT) pattern of HR-TEM image of annealed $CuInSe_2$ nanoparticles illustrates that the particles have quasi-single crystal tetragonal structure, as also confirmed by the XRD pattern. The HR-TEM image clearly shows the fringe widths are in order without any defect with 0.32 nm. Microstructural analysis results clearly indicate that the synthesized and air-annealed nanoparticles are in highly crystalline state with near stoichiometric atomic composition.

Key words: Copper Indium Diselenide (CIS), Nanoparticle, Hot-injection Method, STEM, HR-TEM, XRD

INTRODUCTION

In recent years, the synthesis of nano- and micro-structured semiconductor materials has been extensively studied, since the shape, size, and dimensionality are crucial parameters responsible for their outstanding optoelectronic properties. With the depletion of fossil fuel and challenges of global warming, it becomes evident to utilize alternative sources of energy. Copper indium diselenide (CIS) materials are one of the most promising candidates for thin film photovoltaic applications [1-3]. These chalcogenide compounds ($CuInSe_2$) are extensively researched as a viable candidate for solar energy conversion, primarily due to their high absorption coefficient, suitable band gap, good stability in solar radiation, and facile conversions of n/p carrier type [4]. To date, various methods have been developed for $CuInSe_2$ nanoparticle synthesis, including evaporation [5], spraying [6,7], pyrolysis of molecular single-source precursors [8] and electrodeposition [9]. Notably, Castro and Banger synthesized $CuInSe_2$ nanocrystals by thermal deposition of molecular single-source precursors in a non-coordinating solvent [8]. Guillenmoles et al. [9] reported that $CuInSe_2$ thin film can be prepared by electrodeposition. Malik et al. [10] synthesized mono-dispersed $CuInSe_2$ nanoparticles by reacting tri-*n*-octyl phosphine selenide (TOPSe), CuCl and $InCl_3$ in tri-*n*-octyl phosphine oxide (TOPO). Peng and co-workers obtained $CuInSe_2$ nanowires by Au-catalyzed vapor-liquid-solid (VLS) growth at 700 °C [11]. In general, these techniques usually require either high processing temperatures or special devices, and some of them even use toxic agents such as H_2Se or organometallic compounds.

One of the hurdles currently impeding the widespread commercialization of CIGS-based thin film solar cells is the difficulty in achieving controlled stoichiometry over large device areas, leading to high manufacturing cost and poor device yield [12]. The CIGS layers in state-of-the-art devices are deposited by a multistage co-evaporation technique in which alternate copper, indium, and gallium layers are deposited followed by reacting with a selenium source, Se, or H_2Se gas, in the chamber [13,14]. This process is time-consuming and the CIGS stoichiometry control is rather difficult, resulting in the formation of intermetallic phases. The Se content can also vary significantly in the films made in separate batch [12,15]. Large material losses onto the deposition chamber walls also increase the manufacturing cost. For all of these reasons, alternative CIGS absorber layer deposition strategies are desired. One approach with the potential to produce CIGS layers with controlled stoichiometry without the need for high temperature annealing is to chemically synthesize CIGS nanocrystals with controlled stoichiometry and crystal phase, and disperse them in solvents, creating a paint or ink. Such approaches utilizing printable CIGS inks make them accessible to a wide range of solution-based processing techniques and may lead to inexpensive fabrication routes for CIGS light-absorbing layers [16]. A chemical, solution-based approach alleviates the need for a high temperature annealing step under selenium atmosphere and may solve the CIGS selenium problems, that is, avoiding Se loss and achieving the correct CIGS stoichiometry in films covering large substrate area [17].

Photovoltaic devices incorporating nanocrystal-based CdSe/CdTe [18] and CuS [19] absorber layers have been reported and demonstrated solar energy conversion efficiencies as high as 2.9%, although a high temperature anneal at 400 °C was required. These nanocrystals have also been combined with polymers to produce solution-processed photovoltaics such as hybrid CdSe nanocrystal/poly-3(hexylthiophene) solar cells, which yield reported efficiencies of up to

†To whom correspondence should be addressed.
E-mail: chpark@ynu.ac.kr
‡Present address: Department of Chemistry and Biochemistry, University of Arkansas, Fayetteville, AR 72701, USA

3.2% [20]. Many different semiconductor nanocrystals can be synthesized by colloidal routes, including groups II-VI [21] III-V [22] I-VI [23] and IV-VI [24] semiconductors, but the synthesis of I-III-VI [25] nanocrystals is much less developed. Nonetheless, there are literature reports on the synthesis of ternary chalcopyrite compound nanocrystals, such as $CuInS_2$, $CuInSe_2$, and other I-II-VI [10, 26] semiconductor nanocrystals. These nanocrystals, however, generally suffer from relatively low yields, poor crystallinity [27] and poor uniformity in composition and phase [28]. This is not surprising, considering that many of these systems have very complicated phase diagrams, and nanocrystals can further exhibit greater phase complexity than the corresponding bulk materials [23].

Here, we report a scalable high-yield synthesis solution route of pure phase nanocrystals of chalcopyrite ($CuInSe_2$) with near stoichiometric atomic composition. The nanocrystals disperse readily in various non-polar solvents and can be deposited as uniform, crack-free micrometer-thick films onto the glass or metal substrates. Especially, in this work, the air-annealing effect on the structural, morphological and optoelectronic properties of CIS nanoparticles is investigated.

EXPERIMENTAL

The tri-octyl phosphine (TOP)/tri-octyl phosphine oxide (TOPO) capped CIS nanoparticles were synthesized by using hot-injection method according to the procedure described elsewhere [10].

1. Stock Solution

Se powder (1.66 g) and TOP (20 mL) was stirred at room temperature for 48 h to generate a clear solution (1 M) of TOPSe. The stock solution of Cu-In [CuCl (1.0 g, 1 mmol), $InCl_3$ (2.20 g, 1 mmol) and TOP (15 mL)] was prepared separately at room temperature for 48 h. All chemicals were purchased from Aldrich Company and used without further purification.

2. Preparation of $CuInSe_2$ Nanoparticles

TOPO (20 g) was loaded into the two-neck reaction flask and heated to 100 °C under inert atmosphere for 2 h. After the colorless solution was attained, the stock solution of Cu-In was injected into the hot TOPO at 100 °C. After the Cu-In solution injection, the colorless TOPO turned into bright yellow color, and the temperature dropped to 80 °C. The reaction was allowed to proceed for 1 h, after which the temperature was increased to 250 °C, and then 1 M TOPSe (20 mL) solution was injected into the reaction flask and allowed to proceed for 24 h. The reaction mixture was cooled down to 60 °C, followed by the addition of excess methanol (25 mL) to flocculate the particles which were recovered by centrifugation. The obtained precipitate was washed and centrifuged with methanol to remove excess ligands and then vacuum dried to finally obtain the CIS nanoparticles. The $CuInSe_2$ nanoparticles were then annealed at 320 °C for 10 min in air.

3. Characterization

The structure and chemical composition of $CuInSe_2$ samples were investigated using high resolution transmission electron microscopy (HR-TEM) and scanning transmission electron microscopy (STEM) (Cs-corrected HR-TEM, JEM 2200FS, JEOL). For TEM measurements, the nanoparticles were deposited onto 400-mesh copper Formvar/carbon grids. The crystalline structure of the samples was analyzed by X-ray diffraction by using a Rigaku D/Max-2000 powder diffractometer with Cu$K\alpha$ radiation operating at 40 kV and 100 mA. XPS spectra were recorded by Thermo ESCALAB 250 Instrument with Al $K\alpha$ X-ray as the excitation source. Room temperature PL spectra were obtained by a SPEX 750 M spectrometer using He-Cd laser (excitation wavelength at 325 nm).

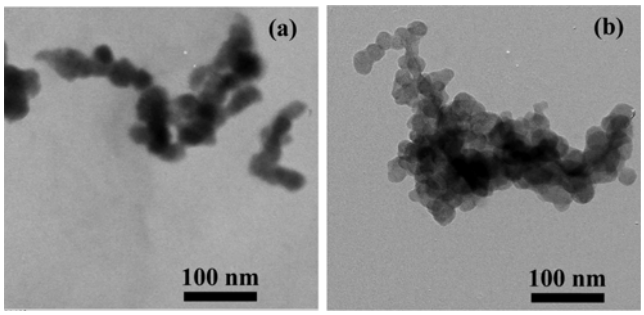

Fig. 1. TEM images of synthesized CIS nanoparticles: (a) as-synthesized nanoparticles; (b) nanoparticles annealed at 320 °C in air for 10 min.

RESULTS AND DISCUSSION

Fig. 1 shows the TEM images of CIS nanoparticles before and after annealing. The average size of the as-synthesized nanoparticles was about 25 nm where organic ligands can also be seen on the periphery of particles (Fig. 1(a)). Annealed particles of approximately the same size did not show organic ligands attached (Fig. 1(b)). The morphology of annealed nanocrystals ($CuInSe_2$) was characterized by HR-TEM as shown in Fig. 2(a) and (b), respectively, a large area high angle annular dark field scanning TEM (HAADF-STEM) image and a bright field (BF) STEM image. The moiety of three particles attached each other was clearly focused. Very clear and sharp crystal structures were observed in a bright field with the visual of crystal lattices. Scanning transmission electron microscopy (STEM) and Atomic number contrast STEM (Z-STEM) use a focused electron beam that is rastered across the sample. The electrons that are scattered at low angles are used to form a bright field image, while those scattered at high angles are used to form a dark field image [29]. Also, it shows a strong atomic number contrast, hence the term Z-STEM or Z-contrast imaging, known as high-angle annular dark field (HAADF) imaging [30-32]. Fig. 2(a) and (b) show the simultaneous Z-STEM (HAADF) and a high-resolution bright field TEM image of a characteristic nanoparticle (25 nm) from the chalcopyrite synthesis and images taken after installation of the aberration corrector. The BF image shows the edge of the nanocrystal more clearly because of the reduced image delocalization, but it is still not able to detect individual atoms on the amorphous carbon support because of the lack of strong Z-contrast. The Z-STEM image does show individual atoms and small clusters on the carbon film. The SAED pattern of corresponding BF image is shown in Fig. 2(c). From the SAED pattern it can be seen that the highly single crystalline nature of the nanoparticles as the spots and crystal faces are clear.

Fig. 2(d) describes the lattice image of the annealed nanoparticles with clear lattice fringes width of 0.3256 nm, which is quite similar to the tetragonal faces. The fast fourier transform (FFT) pat-

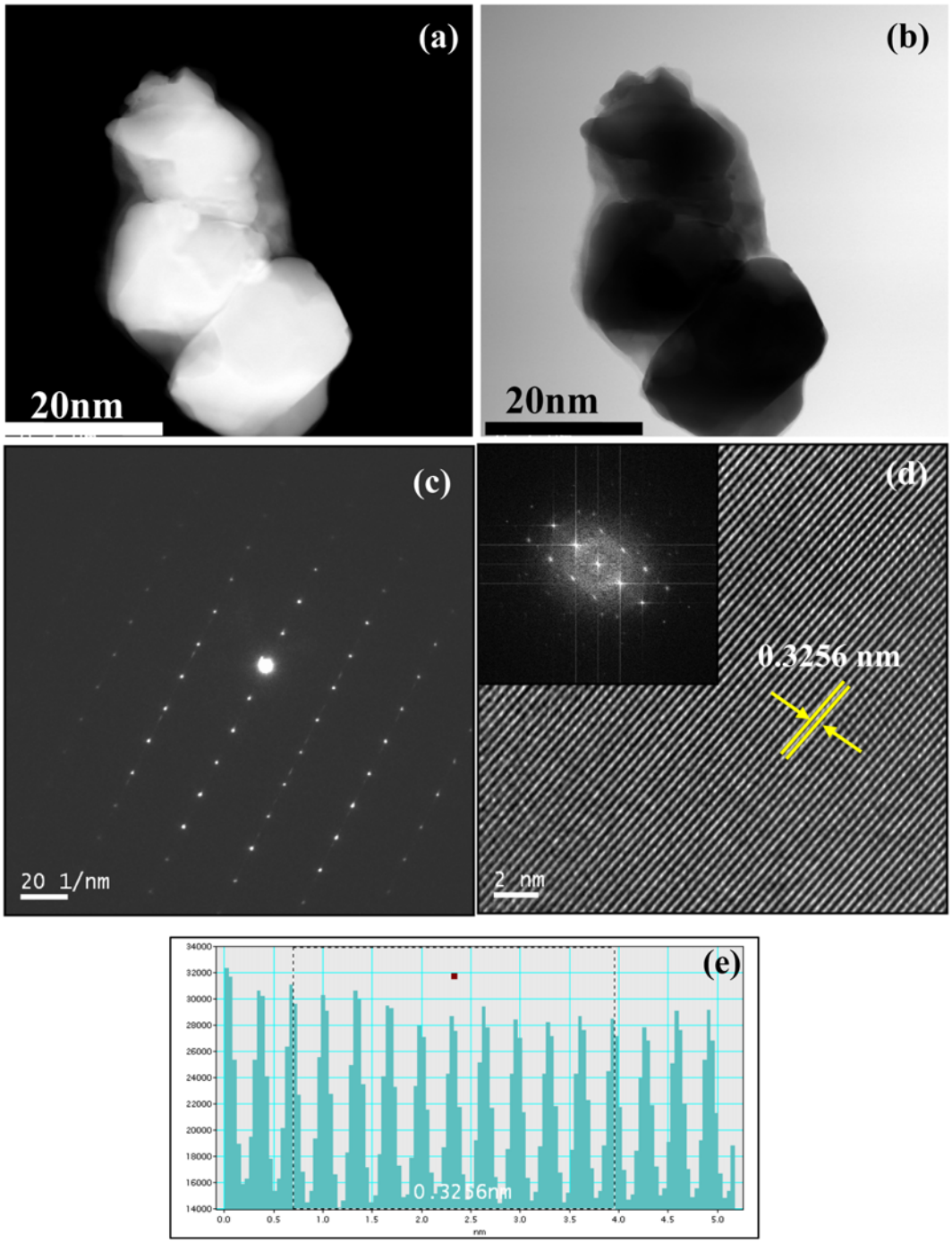

Fig. 2. HR-TEM images of annealed CIS nanoparticles at 320 °C in air for 10 min: (a) high angle annular dark field (HAADF) scanning TEM image; (b) bright field TEM image; (c) corresponding SAED pattern; (d) high resolution TEM images showing the lattice spacing of 0.3256 nm and the corresponding FFT image (inset); (e) profile image of the corresponding HR-TEM image.

tern (inset of Fig. 2(d)) displays clear bright spot lines perpendicular to the lattice fringes, further confirming the growth of particles in tetragonal crystal structure. Fig. 2(e) shows the line profile image of the crystal stacking interlayer, which also corresponds to the tetragonal face. The lattice images indicated that the synthesized nanoparticles are in highly crystalline state along with [112] axis direction; on the other hand, the shape of nanoparticles in our case is not always spherical and exhibits significant faceting. The faceting has thus far been difficult to control, but this might be addressed by the optimization of several factors including the capping ligand chemistry and the way reactants are added to the reaction vessel. Chemical composition of the nanocrystals was analyzed by STEM elemental mapping, which is shown in Fig. 3. The line profile image of nanoparticles in Fig. 2(e) indicated intensity difference between Cu, In and Se atoms, which were also observed by the STEM image, and corresponding EDX elemental mapping of Cu, In and Se (Fig. 3). The elemental mapping clearly shows that the nanoparticles are slightly Se-rich and In-deficient. These observed differences provide addi-

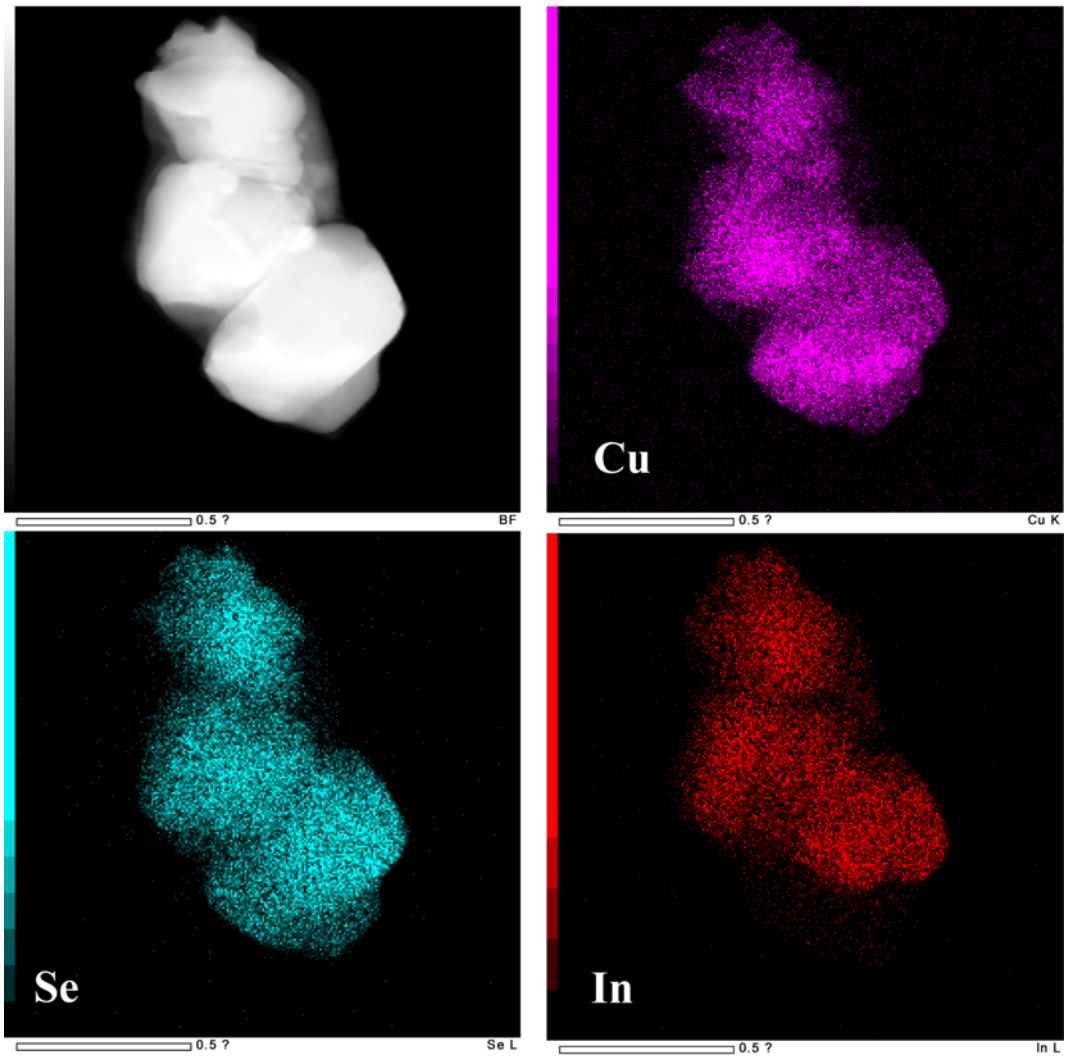

Fig. 3. STEM image and corresponding EDX elemental mapping of Cu, In and Se.

tional evidence of lattice distortion that result from cation ordering and the chalcopyrite crystal structure. Compositional analysis by STEM showed that the average composition of the nanocrystals in the sample has the molar Cu : In : Se ratio of 1 : 1 : 2, and the composition of individual particles measured by EDS characterization were also approximately 1 : 1 : 2 (stoichiometric) with a variation from particle to particle less than the experimental error of ca. 2 at% (figure not shown here), considering that Cu is slightly over represented in the EDS spectra because of the signal from the Cu sample holder. There was no compositional variation from particle to particle within the error of the EDS detector.

Fig. 4 shows the XRD pattern of the synthesized and annealed chalcopyrite CIS nanocrystals. The crystals were very pure, and the intense peak at 2θ=26.6° oriented along [112] direction and peaks at ~44° and ~52° corresponding to the [204/220] and [116/312] crystal planes confirmed that the peaks are consistent with chalcopyrite (body-centered tetragonal structure; JCPDS: 81-1936), and also can be indexed to pure phase of CIS due to the presence of sharp intense peaks. This pattern is in good agreement with the reported features of stoichiometric $CuInSe_2$ with tetragonal phase [33]. No peaks of other impurities were detected, indicating the high purity and crystallinity of CIS samples obtained in this study. The intensities of the peaks were in agreement with the standard pattern, indicating the isotropic nature of the as-prepared particles. Both high-resolu-

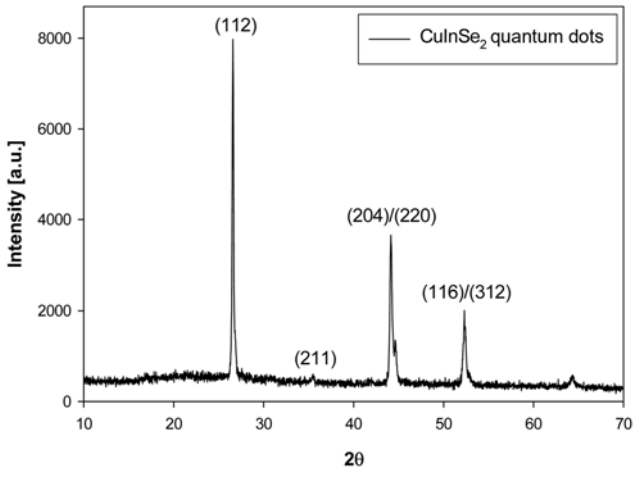

Fig. 4. X-ray diffraction patterns of synthesized CIS nanoparticles.

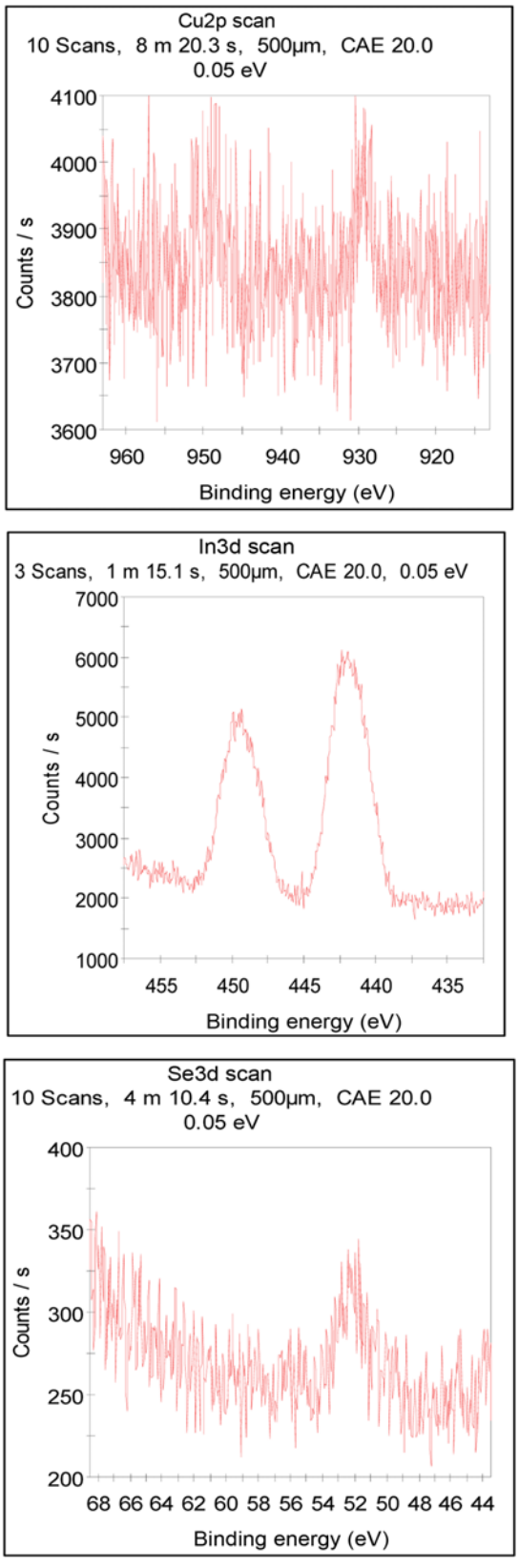

Fig. 5. XPS spectra of synthesized CIS nanoparticles.

tion TEM (Fig. 2) and XRD (Fig. 4) confirmed that the nanocrystals have tetragonal chalcopyrite $CuInSe_2$ structure with approximately 25 nm in size. The *d*-spacings observed in TEM and the FFTs of

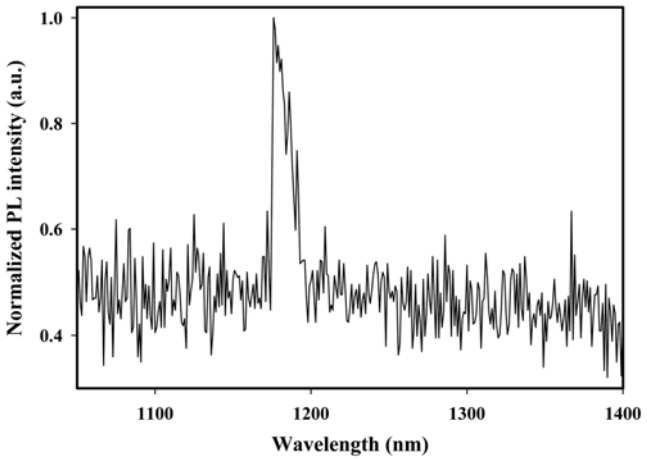

Fig. 6. Room temperature PL spectra of synthesized CIS nanoparticles.

the TEM images are also consistent with the tetragonal $CuInSe_2$ structure, showing no other crystal phases.

XPS spectra of CIS nanoparticles are represented in Fig. 5. The $Cu2p_{3/2}$ band was found to have a binding energy of 930 eV, $In3d_{5/2}$ of 444 eV, and Se3d of 52 eV. The possibility of oxide species is excluded since the binding energy is almost 1 eV higher than copper oxides. Within the resolution of our experiments these energy values agree with existing literature values; however, this result does not completely exclude some contamination of the sample surface with adventitious carbon with the C1s core level binding energy of 284.7 eV, because it can be masked by the relatively intense Se peaking at practically the same energy.

The optical properties of synthesized CIS nanoparticles were determined by photoluminescence (PL) spectra. Fig. 6 shows the room temperature PL spectra of synthesized CIS nanocrystals. The CIS nanoparticles show a dominant PL emission peak at 1.054 eV (1,176 nm), which is slightly blue-shifted of 0.03 eV (35 nm) from the bulk $CuInSe_2$ (1.024 eV; 1,211 nm) counterparts at room temperature [34]. The blue-shift in PL emission was understood by the quantum size effect [35], and the localized states are transferred from deeper localized states to shallower localized states due to the pressure or thermal activation. Further optical studies are required to understand the photonic behavior of synthesized CIS nanocrystals.

The surface of synthesized CIS nanoparticles is expected to be capped by TOPO molecules due to the nature of the well-known hot-injection method. The crystallinity of as-synthesized CIS nanoparticles is improved by thermal annealing (320 °C) in air for 10 min without the change in the nanoparticles' shape, size and optical properties. Annealing also seems to remove the TOPO molecules successfully from the surface of particles without forming significant surface oxides (as revealed in the XPS study), although the possibility of the presence of oxygen in a very thin (undetectable) passivation layer cannot be ruled out [10]. For photovoltaic applications, CIS nanoparticles should have surfaces free from oxides.

CONCLUSIONS

Highly crystalline chalcopyrite $CuInSe_2$ (CIS) nanoparticles with average sizes of approximately 25 nm have been successfully pre-

pared by the hot-injection method. Thermal annealing of the synthesized nanoparticles in air at 320 °C was found to be effective in removing organic ligands from the surface and improving the crystallinity of the particles, without affecting the size and morphology of the particles. HR-TEM studies clearly show that the fringe widths are in order without any defect with 0.32 nm. SAED patterns also show the bright spots in compliance with the highly crystalline nature of the nanoparticles. Particularly, the synthesis method developed in this study could produce CIS nanoparticles in near stoichiometric composition with excellent reproducibility, which can be a benefit in thin film solar cell applications.

ACKNOWLEDGEMENTS

This work was supported by the 2008 Yeungnam University research grant (208-A-345-007), and the Human Resources Development Program of Korea Institute of Energy Technology Evaluation and Planning (KETEP) grant (No. 20104010100580) funded by the Korean Ministry of Knowledge Economy.

REFERENCES

1. D. Cahen, J.-M. Gilet, C. Schmitz, L. Chernyak, K. Gartsman and A. Jakubowicz, *Science*, **258**, 271 (1992).
2. J.-F. Guillemoles, U. R. L. Kronik, H.-W. Schock and D. Cahen, *Adv. Mater.*, **11**, 957 (1999).
3. K. Ramanathan, M. A. Contreras, C. L. Perkins, S. Asher, F. S. Hasoon, J. Keane, D. Young, M. Romero, W. Metzger, R. Noufi, J. Ward and A. Duda, *Progress in Photovoltaics*, **11**, 225 (2003).
4. Y. Y. Han and C. Y. Tsong, *J. Phys. Chem. B*, **110**, 17370 (2006).
5. L. Stolt, J. Hedstrom, J. Kessler, M. Ruckh, K.-O. Velthaus and H.-W. Schock, *Appl. Phys. Lett.*, **62**, 597 (1993).
6. D. L. Schulz, C. J. Curtis, F. A. Flitton, H. Weisner, J. Keane, R. J. Matson, M. J. Jones, P. A. Parilla, R. Noufi and D. S. Ginley, *J. Electron. Mater.*, **27**, 433 (1998).
7. H. Ye, H. S. Park, V. A. Akhavan, B. W. Goodfellow, M. G. Panthani, B. A. Korgel and A. J. Bard, *J. Phys. Chem. C*, **115**, 234 (2011).
8. S. L. Castro, S. G. Bailey, R. P. Raffaelle, K. K. Banger and A. F. Hepp, *Chem. Mater.*, **15**, 3142 (2003).
9. J. F. Guillenmoles, A. Lusson, P. Cowache, S. Massaccesi, J. Vedel and D. Lincot, *Adv. Mater.*, **6**, 376 (1994).
10. M. A. Malik, P. O'Brien and N. Revaprasadu, *Adv. Mater.*, **11**, 1441 (1999).
11. H. Peng, D. T. Schoen, S. Meister, X. F. Zhang and Y. Cui, *J. Am. Chem. Soc.*, **129**, 34 (2007).
12. M. Powalla and B. Dimmler, *Thin Solid Films*, **361-362**, 540 (2000).
13. I. Repins, M. A. Contreras, B. Egaas, C. DeHart, J, Scharf, C. L. Perkins, B. To and R. Noufi, *Prog. PhotoVoltaics Res. Appl.*, **16**, 235 (2008).
14. M. A. Contreras, B. Egaas, K. Ramanathan, J. Hiltner, A. Swartzlander, F. Hasoon and R. Noufi, *Prog. PhotoVoltaics Res. Appl.*, **7**, 311 (1999).
15. H.-W. Schock and R. Noufi, *Prog. PhotoVoltaics Res. Appl.*, **8**, 151 (2000).
16. C. Eberspacher, K. L. Pauls and J. P. Serra, *Mater. Res. Soc. Symp. Proc.*, **763**, B8.27.1 (2003).
17. A. P. Kumar and K. V. Reddy, *Thin Solid Films*, **304**, 365 (1997).
18. I. Gur, N. A. Fromer, M. L. Geier and A. P. Alivisatos, *Science*, **310**, 462 (2005).
19. Y. Wu, C. Wadia, W. Ma, B. Sadtler and A. P. Alivisatos, *Nano Lett.*, **8**, 2551 (2008).
20. S. Dayal, N. Kopidakis, D. C. Olson, D. S. Ginley and G. Rumbles, *J. Am. Chem. Soc.*, **10**, 239 (2010).
21. C. B. Murray, D. J. Norris and M. G. Bawendi, *J. Am. Chem. Soc.*, **115**, 8706 (1993).
22. O. I. Micic, C. J. Curtis, K. M. Jones, J. R. Sprague and A. J. Nozik, *J. Phys. Chem.*, **98**, 4966 (1994).
23. A. Ghezelbash and A. Korgel, *Langmuir*, **21**, 9451 (2005).
24. J. Xu, J.-P. Ge and Y.-D. Li, *J. Phys. Chem. B*, **110**, 2497 (2006).
25. J. D. Holmes, K. J. Ziegler, R. C. Doty, L. E. Pell, K. P. Johnston and B. A. Korgel, *J. Am. Chem. Soc.*, **123**, 3743 (2001).
26. X. Lu, B. A. Korgel and K. P. Johnston, *Chem. Mater.*, **17**, 6479 (2005).
27. C. Eberspacher, K. Pauls and J. Serra, 28th IEEE Photovoltaic Specialist Conference, IEEE, 517 (2000).
28. S.-H. Choi, E.-G. Kim and T. Hyeon, *J. Am. Chem. Soc.*, **128**, 2520 (2006).
29. O. L. Krivanek, P. D. Nellist, N. Dellby, M. F. Murfitt and Z. Szilagyi, *Ultramicroscopy*, **96**, 229 (2003).
30. A. V. Kadavanich, T. C. Kippeny, M. M. Erwin, S. J. Pennycook and S. J. Rosenthal, *J. Phys. Chem. B*, **105**, 361 (2001).
31. P. D. Nellist and S. J. Pennycook, *Ultramicroscopy*, **78**(1-4), 111 (1999).
32. S. J. Pennycook and P. D. Nellist, Z-Contrast Scanning Transmission Electron Microscopy, in: D. Rickerby, G. Valdre, U. Valdre (Eds.), Impact of Electron Scanning Probe Microscopy on Materials Research, Kluwer Academic Publishers, The Netherlands (1999).
33. B. Li, Y. Xie, J. Huang and Y. Qian, *Adv. Mater.*, **11**, 1456 (1999).
34. S. Chichibu, T. Mizutani, K. Murakami, T. Shioda and T. Kurafuji, *J. Appl. Phys.*, **83**, 3678 (1998).
35. Q. Guo, S. J. Kim, M. Kar, W. N. Shafarman, R. W. Birkmire, E. A. Stach, R. Agrawal and H. W. Hillhouse, *Nano Lett.*, **8**, 2982 (2008).